

**This item is the archived peer-reviewed author-version of:**

High Chern number in strained thin films of dilute magnetic topological insulators

**Reference:**

Shafiei Mohammad, Fazileh Farhad, Peeters François, Milošević Milorad.- High Chern number in strained thin films of dilute magnetic topological insulators  
Physical review B / American Physical Society - ISSN 2469-9969 - 107:19(2023), 195119  
Full text (Publisher's DOI): <https://doi.org/10.1103/PHYSREVB.107.195119>  
To cite this reference: <https://hdl.handle.net/10067/1972950151162165141>

# High Chern number in strained thin films of dilute magnetic topological insulators

Mohammad Shafiei,<sup>1,2</sup> Farhad Fazileh,<sup>1</sup> François M. Peeters,<sup>2</sup> and Milorad V. Milošević<sup>2,3,\*</sup>

<sup>1</sup>*Department of Physics, Isfahan University of Technology, Isfahan 84156-83111, Iran*

<sup>2</sup>*Department of Physics, University of Antwerp, Groenenborgerlaan 171, B-2020 Antwerp, Belgium*

<sup>3</sup>*NANOlaboratory Center of Excellence, University of Antwerp, Belgium*

(Dated: July 6, 2023)

The quantum anomalous Hall effect was first observed experimentally by doping Bi<sub>2</sub>Se<sub>3</sub> materials family by chromium, where 5% doping induces an exchange field of around 0.1 eV. In ultra-thin films, a topological phase transition from normal insulator to a Chern insulator can be induced with an exchange field proportional to the hybridization gap. Subsequent transitions to states with higher Chern numbers require exchange field larger than the (bulk) band gap, but are prohibited in practice by detrimental effects of higher doping levels. Here we show that threshold doping for these phase transitions in thin films is controllable by strain. As a consequence, higher Chern states can be reached with experimentally feasible doping, sufficiently dilute for the topological insulator to remain structurally stable. Such facilitated realization of higher Chern insulators opens prospects for multi-channel quantum computing, higher-capacity circuit interconnects, and energy-efficient electronic devices at elevated temperatures.

Following the discovery of topological insulators (TIs), the potential of these materials as a platform for the exploration of novel quantum phenomena, such as topological superconductivity, quantum anomalous Hall (QAH) insulators, and spintronic capabilities, was extensively examined [1]. The best known 3D TI is Bi<sub>2</sub>Se<sub>3</sub>, with a bulk gap of 0.29 eV and a rhombohedral layered structure (with structural  $\frac{c}{a}$  ratio of 6.921), in which each unit-cell contains five atomic layers [referred to as a quintuple layer (QL)] with covalent intralayer interactions and van der Waals interlayer interactions [2–7]. Bi<sub>2</sub>Se<sub>3</sub> has been subject to very many investigations to date, and is considered a candidate for viable technological applications. One should note however that developing devices using TIs is more challenging than using typical semiconductors. The three challenges of the presence and protection of surface states, bulk being insulating, and the controllability of these surface states, all must be considered simultaneously while constructing TI devices [8, 9]. Given these challenges, the development of thin-film TIs has attracted more attention due to the facilitated control of TI characteristics. Topological surface states are primarily regulated by gating, proximity effect, and size-quantization effects [1], while TI characteristics can be controlled, for example, by selecting a suitable substrate. Overlap between top and bottom surface states in thin materials enables quantum tunneling between these states and induces a hybridization gap [10, 11]. The hybridization gap closes as the thickness of the material is increased, forming a Dirac cone [12, 13]. Thin-film Bi<sub>2</sub>Se<sub>3</sub> can be accurately grown, QL-by-QL, using molecular beam epitaxy [13].

QAH effect occurs when the time-reversal symmetry (TRS) is broken by an exchange field, such as magnetization, in the absence of a magnetic field, and Hall conductance becomes  $\sigma_{xy} = C \frac{e^2}{h}$  where the invariant  $C$  is the Chern number [14–16]. Because of the unique

topological properties of these states, efforts have been made to introduce materials and conditions in which the QAH effect may be observed, in systems such as Rashba-graphene coupled with exchange field [16], optical lattice model [17], Anderson insulator [18], and magnetic TIs [15]. The topological band structure of TIs with strong spin-orbit coupling (SOC) was later revealed to be an ideal platform for researching QAH states, particularly when doped with Cr or Fe [19]. However, identifying QAH states in magnetic TI films experimentally is challenging and requires special conditions such as long-range ferromagnetic order and controllable film thickness - because the dissipative conduction electrons must be localized, the exchange field must be larger than the hybridization gap, and the Fermi energy must be within the gap [20, 21]. In addition, the easy magnetization axis should be perpendicular to the film plane, and magnetic impurities aligned accordingly [22–24]. Despite these many demands, QAH states were successfully observed in Cr- and V-doped (Bi<sub>x</sub>Sb<sub>1-x</sub>)<sub>2</sub>Te<sub>3</sub> [25, 26], with  $x = 0.1 - 0.3$ . Rare-earth element doping of TIs, such as by Eu [27], is also of major interest due to the larger magnetic moment and gap compared to doping by transition metal elements [28]. Of course, only dilute doping is permitted since the Fermi energy is placed inside the gap, whereas at high concentrations, SOC is attenuated, resulting in the loss of surface states in TI [29]. Alternatively, one can explore QAH states in TIs proximitized to magnetic insulators, which also breaks the TRS and induces magnetization. In either case, for ultra-thin film the Hall conductance is initially zero, but as the magnetization rises beyond a critical value that is proportional to the hybridization gap, the Chern number becomes one, signifying the topological phase transition to a Chern insulator.

The Chern number is computed as the integral of the Berry curvature on the first Brillouin zone, and deter-

mines the number of chiral edge channels in the sample [30]. In recent years, the attention of the community has turned to systems with Chern number *higher than 1*, enabling larger number of topological Fermi-arc surface states [31], larger number of Landau levels involved in magnetotransport [32], larger magnitude of photocurrent in the photogalvanic effect [33], and multimode photonic waveguides [34]. Contact resistance between electrodes and chiral channels is restricted to  $h/e^2$  in insulators with  $C = 1$ , and having insulators with  $C > 1$  alleviates this constriction and reduces the resistance [35, 36]. Furthermore, as  $C > 1$  increases the effective breakdown current, the practical application of these insulators in QAH devices becomes more feasible [36, 37].

High Chern number should be seemingly achievable in thin-film TIs by increasing the exchange field related to magnetic dopants [15]. However, there are practical constraints to doping magnetic atoms into the system, since increased doping can shift the Fermi energy outside the bulk band gap or cause disorder that harms the material structure and increases scattering [21]. It is therefore unlikely to reach high Chern states experimentally in this manner, since required doping levels are high. In this Letter, we demonstrate that it is indeed possible to achieve high Chern states at sufficiently low concentration of magnetic dopants, if TI properties are tailored using strain. We detail the Chern phase diagram for magnetically-doped  $\text{Bi}_2\text{Se}_3$  film as a function of its thickness, doping magnetization, and applied strain, and discuss the effect of doping distribution on the found topological transitions, all to facilitate the experimental realization of the high-Chern states in this system.

As mentioned, we will consider a magnetically-doped  $\text{Bi}_2\text{Se}_3$  film of thickness expressed as a number of quintuple layers  $N_{QL}$ . Each site is considered as a lattice site with four states  $\{|P1 \uparrow\rangle, |P2 \uparrow\rangle, |P1 \downarrow\rangle, |P2 \downarrow\rangle\}$ , where P1 and P2 denote the orbitals and  $\uparrow\downarrow$  the spin. One usually considers dilute magnetic impurities and defines their concentration as  $n_{imp} = (N_{imp}/N)$ , in which  $N_{imp}$  impurities are randomly distributed over  $N$  lattice sites and should build special quasi-random structures. Since the size of all magnetic impurities is the same in our consideration, as is the orientation of their magnetic moments, we add the effect of magnetic impurities to the Hamiltonian solely via the exchange field [38]. For example, 5% Cr doping of  $\text{Bi}_2\text{Se}_3$  ( $\text{Cr}_x(\text{Bi}_2\text{Se}_3)_{1-x}$ ) in experiment corresponds to an exchange field of around 0.1 eV [19] [39]. Magnetic dopants in TIs can substitute only the metal atoms [40] or be dispersed across all lattice sites [41, 42], and we consider the latter scenario. The effective real-space tight-binding Hamiltonian for magnetically-doped  $\text{Bi}_2\text{Se}_3$  is defined as follows [43, 44]:

$$H = \sum_i c_i^\dagger E c_i + \sum_{i,\alpha} (c_i^\dagger T_\alpha c_{i+\alpha} + h.c.) + \sum_i c_i^\dagger M c_i, \quad (1)$$

where the last term describes magnetic doping (such as Cr, Fe, Ti, or V), with the resulting exchange field de-

noted by  $M$ . In the preceding terms in Eq. (1),  $E$  and  $T_\alpha$  are  $4 \times 4$  matrices for onsite energy and hopping parameters between unit cells, respectively. The hopping parameters were determined by comparing the band structure of the effective Hamiltonian to the DFT data [45] near the  $\Gamma$  point [24].

In thin films, strain is known to strongly affect the surface states in  $\text{Bi}_2\text{Se}_3$  [46, 47], as experimentally observed near the grain boundaries [48], or in the vicinity of substitution sites with heavier atoms (such as Te), hence it presents an effective method for engineering band gap and tuning Dirac states. One should note that applying a uniform in-plane biaxial strain in the  $\text{Bi}_2\text{Se}_3$  family of materials is rather challenging experimentally. As these are layered van der Waals materials, when thin films are grown on a substrate with a lattice mismatch, the lattice constant in the layers adjacent to the interface immediately relaxes to the bulk value, and no apparent strain arises [49]. Assuming that these practical challenges can be overcome, in what follows we will consider uniform strain of magnetically-doped  $\text{Bi}_2\text{Se}_3$  films, both vertical uniaxial and in-plane biaxial one, defined as  $\varepsilon_\perp = (c - c_0)/c_0$  and  $\varepsilon_\parallel = (a - a_0)/a_0$  respectively, where  $a_0 = 4.138 \text{ \AA}$  and  $c_0 = 28.64 \text{ \AA}$  are lattice constants for unstrained  $\text{Bi}_2\text{Se}_3$ . The two strains are linked through the Poisson ratio  $\nu = \frac{\varepsilon_\perp}{\varepsilon_\perp - 2\varepsilon_\parallel}$  [50], which is 0.29 for  $\text{Bi}_2\text{Se}_3$  [51]. If  $\mathbf{u}_\alpha$  is the displacement of the lattice point along the  $\mathbf{x}_\beta$  axis, the strain tensor is expressed as  $\varepsilon_{\alpha,\beta} = \frac{\partial \mathbf{u}_\alpha}{\partial \mathbf{x}_\beta}$ , ( $\mathbf{u}_\alpha = \mathbf{u}_x, \mathbf{u}_y, \mathbf{u}_z$ ,  $\mathbf{x}_\beta = \mathbf{x}, \mathbf{y}, \mathbf{z}$ ). Based on the symmetries of the  $\text{Bi}_2\text{Se}_3$  structure, the strain Hamiltonian becomes [52, 53]

$$\begin{aligned} H_{strain} = & (D_1 \varepsilon_\perp + D_2 \varepsilon_\parallel) \sigma_z \otimes \sigma_0 \\ & + (D_{21} \varepsilon_\perp + D_{22} \varepsilon_\parallel) \sigma_x \otimes \sigma_x + i(D_{21} \varepsilon_\perp + D_{22} \varepsilon_\parallel) \sigma_x \otimes \sigma_y \\ & + (D_{11} \varepsilon_\perp + D_{12} \varepsilon_\parallel) \sigma_x \otimes \sigma_z. \end{aligned} \quad (2)$$

Parameters  $D_1$  and  $D_2$  and the Poisson ratio determine the hybridization gap and the bulk gap of the TI based on the symmetry group, and the values for these parameters are extracted from Refs. [46, 53] and available DFT data as  $D_1 = -2.635 \text{ eV}$ ,  $D_2 = 2.141 \text{ eV}$ . The remaining parameters  $D_{21} = 1.0 \text{ eV}$ ,  $D_{22} = -0.8 \text{ eV}$ ,  $D_{11} = 1.25 \text{ eV}$ , and  $D_{12} = -1.0 \text{ eV}$  we approximated using the Harrison rule [54].

The system is investigated in two regimes: (i) the ultrathin film, having a hybridization gap, and (ii) the thin-film regime, without any hybridization gap. By decreasing the thickness of the TI to a few nanometers, the surface states on the top and bottom surfaces overlap and hybridize by quantum tunneling, causing the hybridization gap to open in the surface states. For 2-6 QL thicknesses, the hybridization gap in our model is 110, 70, 45, 25, and 10 meV, respectively [44]. The molecular beam epitaxy can be used to precisely regulate the film's thickness, and the dependence of QAH states on film thickness could be experimentally investigated [55]. In the ultra-

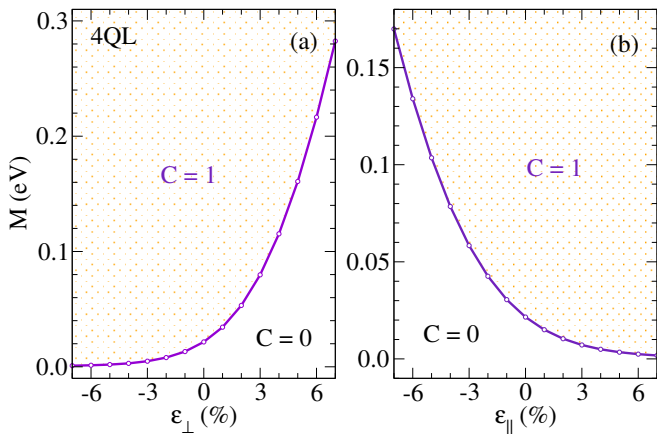


FIG. 1. Phase transition from a normal insulator to a Chern insulator in a magnetically-doped ultra-thin film of  $\text{Bi}_2\text{Se}_3$  ( $N_{QL} = 4$ ). Exchange field as a function of (a) out-of-plane strain, and (b) biaxial in-plane strain. In either case all lattice constants are adjusted according to the Poisson ratio of  $\text{Bi}_2\text{Se}_3$ .

thin film regime, an exchange magnetization greater than the hybridization gap induces a transition from normal insulator ( $C = 0$ ) to a Chern insulator ( $C = 1$ ). In this regime, applying a tensile uniaxial strain in the out-of-plane ( $z$ ) direction causes the hybridization gap to grow. Conversely, when a compressive vertical strain is applied, the hybridization gap decreases and finally closes. Being connected through Poisson ratio, the behavior of the system under strain applied in-plane mirror reflects the behavior under applied vertical strain. As a result, shown in Fig. 1 for the 4QL sample, one is able to control the hybridization gap by applying strain to the system and to regulate the phase transition from  $C = 0$  to  $C = 1$  for different doping concentrations.

In the thin-film regime, a small magnetization leads to the breaking of time-reversal symmetry and opens a gap in the Dirac cone, bringing the system into the  $C = 1$  phase [44]. For  $C > 1$  to be observed, the thickness of the system must be sufficient to have no hybridization gap, and the gap due to magnetization must be larger than the bulk gap of the system. At every transition to a state with higher Chern number, the bulk band gap closes when the exchange field reaches the critical value, the new chiral edge channel forms, and new bulk gap establishes [15]. The latter is then decreased again when the exchange field is increased towards the next critical value for the Chern number to increase by 1. Given that the rise in magnetization by doping is restricted by structural stability of the host material, we opt to instead reduce the bulk gap of the system by strain to achieve the states with higher Chern number for moderate magnetization values. We note that the gaps in the surface-state behave opposite to the bulk gap as a function of strain [53]. As a result, we show in Fig. 2 for a film of

$N_{QL} = 12$  that transition  $C = 0$  to  $C = 1$  is unaltered by strain, but transition to a Chern number 2 becomes possible with increasing magnetic doping - where threshold magnetization for  $C = 1$  to  $C = 2$  transition can be decreased to experimentally accessible values by applying appropriate strain to tune the bulk gap. One should notice that in this case strain can be used to induce a topological transition from a state with  $C = 1$  to a state with  $C > 1$  (and vice versa), in a sample with fixed concentration of the dopants. Note that in the ultra-thin film regime, applying strain to reduce the hybridization gap causes the bulk gap to rise, making it impossible to obtain states with high Chern numbers.

Our calculated threshold values of magnetization for phase transitions to higher Chern number states are summoned in Fig. 3, for films of thickness  $N_{QL} = 2 - 16$ , with and without strain [56]. Two regimes of behavior are clearly seen, with ultra-thin one persisting for  $N_{QL} < 6$ , and the thin-film regime for  $N_{QL} > 6$ . In the ultra-thin regime, the adjustment of the hybridization gap as described in Fig. 1 with strain is stronger for thinner samples. The threshold magnetization for the  $C = 0 \rightarrow 1$  phase transition decreases with thickness, and is decreased by compressive out-of-plane strain (i.e. tensile in-plane strain). In the thin-film regime, the threshold magnetization for  $C = K \rightarrow K + 1$  transitions to high-Chern number states also decreases with sample thickness, but is further lowered by tensile out-of-plane strain (i.e. compressive in-plane strain).

Note that in the transition region of thicknesses  $N_{QL} = 6 - 8$  both behaviors are simultaneously seen. For  $N_{QL} > 13$  the effect of strain no longer changes with the sample thickness, indicating bulk behavior. Notably, in this regime the  $C = 2$  state is reached with exchange magnetization below 0.1 eV, an experimentally achievable value

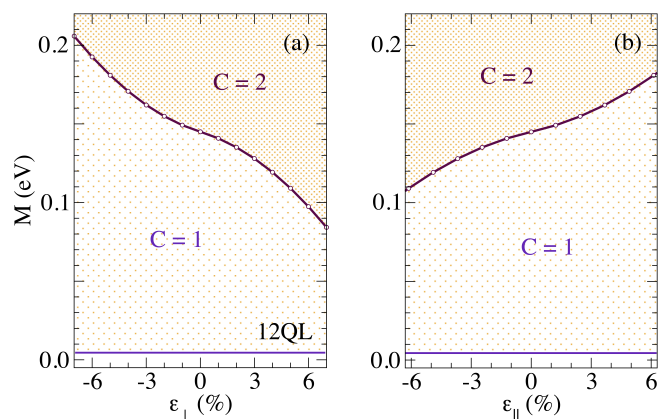


FIG. 2. Phase transition from a Chern insulator with  $C = 1$  to one with  $C > 1$  in a magnetically-doped thin film of  $\text{Bi}_2\text{Se}_3$  ( $N_{QL} = 12$ ). Exchange field as function of (a) out-of-plane strain, and (b) biaxial in-plane strain, at experimentally acceptable doping values.

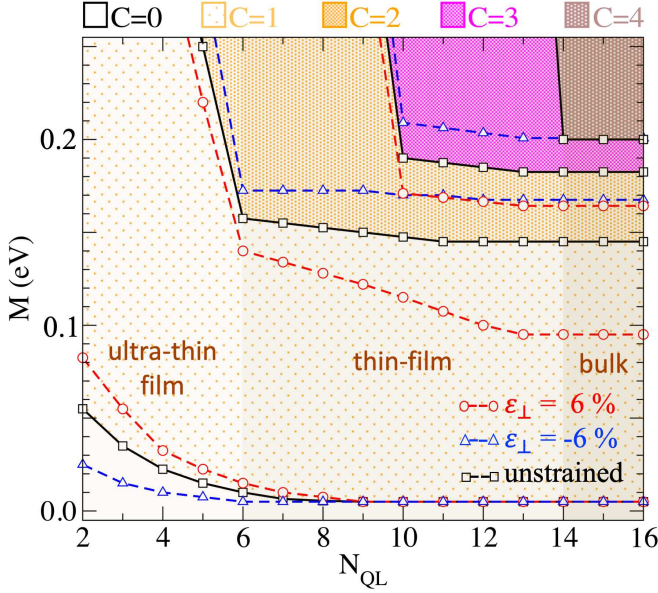


FIG. 3. The Chern phase diagram as a function of the film thickness, the magnetization due to doping, and the applied strain. Shaded areas correspond to changing Chern numbers in the unstrained case.

in a dilute magnetically-doped  $\text{Bi}_2\text{Se}_3$  film [19, 57]. In this regime, large Chern numbers  $C \geq 4$  may be achieved with exchange fields greater than 0.2 eV.

The above findings can be conveniently validated through transport measurements, readily used for identifying and characterizing TIs [1]. Therefore, to validate the above findings through expected quantum Hall effects, we calculate the conductance using the Landauer-Büttiker formalism at zero temperature [58]:

$$G = \frac{e^2}{h} \text{tr}[\Gamma_L(E) G^R(E) \Gamma_R(E) G^A(E)], \quad (3)$$

where

$$\Gamma_{L(R)} = i[\Sigma_{L(R)}(E) - i\Sigma_{L(R)}^\dagger(E)], \quad (4)$$

describes the coupling of the device to the leads L(R) and can be expressed in terms of a self-energy  $\Sigma_{L(R)}$ .  $G^{R(A)}(E)$  is the retarded (advanced) Green's function defined as:

$$\begin{aligned} G^R(E) &= [E - H_D - \Sigma_L^R(E) - \Sigma_R^R(E)]^{-1}, \\ G^A(E) &= [G^R(E)]^\dagger. \end{aligned} \quad (5)$$

Here  $\Sigma_{L(R)}$  can be considered as an effective Hamiltonian describing the lead-device interaction [59]. Fig. 4(a) shows the calculated influence of exchange field strength on the Hall conductance for samples of various thicknesses, and fully corroborates the phase diagram shown in Fig. 3. For example,  $M = 0.05$  eV is smaller than the threshold value of the  $C = 0 \rightarrow 1$  phase transition for 2QL film, hence the conductance for  $N_{\text{QL}} = 2$  is zero

(corresponding to  $C = 0$ ), but becomes  $e^2/h$  for samples thicker than 2QL. For samples with a thickness of 2-17 QL,  $C$  equals one when  $M = 0.1$  eV, and conductance is indeed constant. High Chern numbers can be observed by increasing the exchange field value beyond the bulk band gap, and our calculated quantized conductance follows accordingly. In Fig. 4(b) we show the calculated Hall conductance for  $M = 0.1$  eV, which is equivalent to 5% Cr-doping of  $\text{Bi}_2\text{Se}_3$ , in the presence of strain. As a function of film thickness, we again confirm that high Chern numbers become reachable for reasonably large tensile (compressive) out-of-plane (in-plane) strain - in accordance with the phase diagram shown in Fig. 3.

Finally, we reiterate that introducing magnetic dopants into a topological thin film poses unwanted challenges because they can cause a shift in Fermi energy beyond the bulk bandgap or present a strong disordering effect that leads to magnetic and nonmagnetic scattering. If present as dopants, magnetic atoms can be localized within the surface layers or dispersed deeper within the TI bulk. Surface doping preserves the TI properties of the bulk material. Note however that the surface states wave functions of  $\text{Bi}_2\text{Se}_3$  are not confined to the first QL and have a penetration depth of around 4QL [24]. Therefore, to check the robustness of our findings to the distribution of the magnetic dopants in the TI film, we calculated the Hall conductance for the dopants localized at surfaces and for the same amount of dopants dispersed across the film of thickness 12QL, as presented in Fig. 5. Next to the weak deviation from the quantized value due to edge effects in our calculations [44], we note that introducing magnetic moments to the bulk of the TI causes the

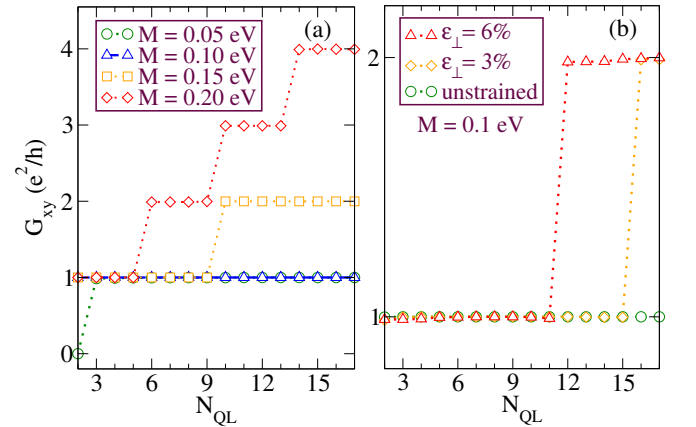


FIG. 4. (a) The effect of magnetic dopants on Hall conductance ( $G_{xy}$ ) as a function of film thickness and exchange field strength. A phase transition to states with higher Chern numbers is found with increasing film thickness and exchange field beyond a minimum of 0.29 eV. (b) The Hall conductance as a function of film thickness, for two values of tensile out-of-plane strain, demonstrating that a high Chern number ( $C > 1$ ) can be achieved at a relatively low exchange field of  $M = 0.1$  eV.

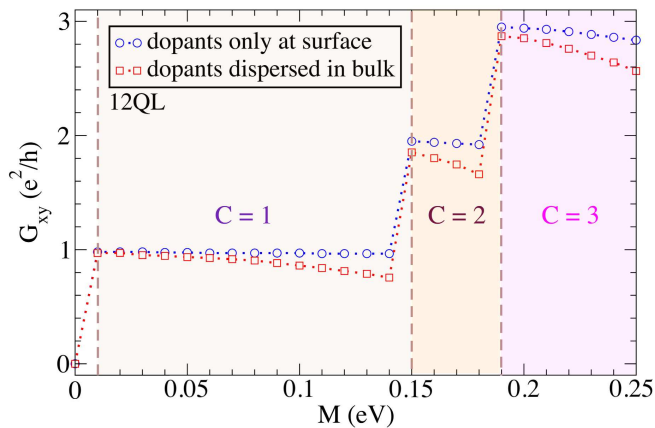


FIG. 5. Effects of bulk and surface doping on Hall conductance for different magnetization for an unstrained sample with thickness  $N_{QL} = 12$ . The detrimental effects of bulk doping on Hall conductance are enhanced by increasing the exchange field of the magnetic dopants, but the Chern number remains unaltered compared to the surface doping case.

Hall conductance to deviate more from the exact quantized value than for the magnetic moments only present at the surface, due to the so-called detrimental bulk effect, readily observed as a function of thickness in [60]. Namely, magnetic dopants dispersed in bulk may scatter and increase the localization of surface states, which leads to an increase in Hall resistance (decrease in Hall conductance). In either case however, the number of chiral channels does not vary and the Chern number remains preserved.

To conclude, the large magnetization required to produce QAH states is one of the main obstacles to realize these states. We showed that using magnetic dopants in combination with applied strain one can tune the hybridization gap in a TI film and regulate the phase transition from trivial  $C = 0$  to topological  $C = 1$  state in the ultra-thin-film regime. In the thin-film regime the nontrivial topological state is reached already at any low magnetization, but we demonstrated that strain can serve to tailor the bulk gap in a way that transitions to states with *higher* Chern numbers ( $C \geq 2$ ) become feasible at experimentally achievable doping levels. Our approach and conclusions are universal for the  $\text{Bi}_2\text{Se}_3$  family of materials ( $\text{Bi}_2\text{Se}_3$ ,  $\text{Bi}_2\text{Te}_3$ ,  $\text{Sb}_2\text{Te}_3$ ) and odd septuple layers of the  $\text{MnBi}_2\text{Se}_4$  family ( $\text{MnBi}_2\text{Se}_4$ ,  $\text{MnBi}_2\text{Te}_4$ ), which correspond to the symmetry group No. 166, in all of which we thus expect high Chern number states to be accessible with strain at lower concentration values of magnetic doping. Our findings thereby enable practical realization of QAH states with high Chern number that are usually evasive, while their reduced resistance is highly-sought after for applications in higher-capacity circuit interconnects and energy-efficient elec-

tronic devices [21]. In addition, high-Chern QAH states in magnetic TIs in heterostructures with superconductors are expected to host zero fermion modes - for use in multi-channel quantum computation [61, 62].

This research was supported by the Research Foundation-Flanders (FWO-Vlaanderen), the FWO-FNRS EoS-ShapeME project, the Isfahan University of Technology, and the Iran Science Elites Federation.

\* [milorad.milosevic@uantwerpen.be](mailto:milorad.milosevic@uantwerpen.be)

- [1] O. Breunig and Y. Ando, *Nature Reviews Physics* **4**, 184 (2022).
- [2] Y. Xia, D. Qian, D. Hsieh, L. Wray, A. Pal, H. Lin, A. Bansil, D. Grauer, Y. S. Hor, R. J. Cava, and M. Z. Hasan, *Nature Physics* **5**, 398 (2009).
- [3] T. Zhang, P. Cheng, X. Chen, J.-F. Jia, X. Ma, K. He, L. Wang, H. Zhang, X. Dai, X. X. Fang, Zhong, and Q.-K. Xue, *Physical Review Letters* **103**, 266803 (2009).
- [4] Y. Chen, J. G. Analytis, J.-H. Chu, Z. Liu, S.-K. Mo, X.-L. Qi, H. Zhang, D. Lu, X. Dai, and Z. Fang, *Science* **325**, 178 (2009).
- [5] S. S. Hong, W. Kundhikanjana, J. J. Cha, K. Lai, D. Kong, S. Meister, M. A. Kelly, Z.-X. Shen, and Y. Cui, *Nano Letters* **10**, 3118 (2010).
- [6] W. Liu, X. Peng, C. Tang, L. Sun, K. Zhang, and J. Zhong, *Physical Review B* **84**, 245105 (2011).
- [7] H. Zhang, C.-X. Liu, X.-L. Qi, X. Dai, Z. Fang, and S.-C. Zhang, *Nature Physics* **5**, 438 (2009).
- [8] F. Munzing, O. Breunig, H. F. Legg, S. Roitsch, D. Fan, M. Rosler, A. Rosch, and Y. Ando, *Nature Communications* **12**, 1038 (2021).
- [9] S. Cho, B. Dellabetta, R. Zhong, J. Schneeloch, T. Liu, G. Gu, M. J. Gilbert, and N. Mason, *Nature Communications* **6**, 7634 (2015).
- [10] C.-X. Liu, H. Zhang, B. Yan, X.-L. Qi, T. Frauenheim, X. Dai, Z. Fang, and S.-C. Zhang, *Physical Review B* **81**, 041307 (2010).
- [11] T. Oh, *Scientific Reports* **10**, 9509 (2020).
- [12] H.-Z. Lu, W.-Y. Shan, W. Yao, Q. Niu, and S.-Q. Shen, *Physical Review B* **81**, 115407 (2010).
- [13] Y. Zhang, K. He, C.-Z. Chang, C.-L. Song, L.-L. Wang, X. Chen, J.-F. Jia, Z. Fang, and Dai, *Nature Physics* **6**, 584 (2010).
- [14] F. D. M. Haldane, *Physical Review Letters* **61**, 2015 (1988).
- [15] H. Jiang, Z. Qiao, H. Liu, and Q. Niu, *Physical Review B* **85**, 045445 (2012).
- [16] Z. Qiao, S. A. Yang, W. Feng, W.-K. Tse, J. Ding, Y. Yao, J. Wang, and Q. Niu, *Physical Review B* **82**, 161414 (2010).
- [17] C. Wu, *Physical Review Letters* **101**, 186807 (2008).
- [18] C.-X. Liu, X.-L. Qi, X. Dai, Z. Fang, and S.-C. Zhang, *Physical Review Letters* **101**, 146802 (2008).
- [19] R. Yu, W. Zhang, H.-J. Zhang, S.-C. Zhang, X. Dai, and Z. Fang, *Science* **329**, 61 (2010).
- [20] K. Nomura and N. Nagaosa, *Physical Review Letters* **106**, 166802 (2011).
- [21] K. He, Y. Wang, and Q.-K. Xue, *Annual Review of Condensed Matter Physics* **9**, 329 (2018).

- [22] N. Pournaghavi, M. Islam, R. Islam, C. Autieri, T. Dietl, and C. M. Canali, *Physical Review B* **103**, 195308 (2021).
- [23] R. ISLAM, S. Mardanya, A. Lau, G. Cuono, T.-R. Chang, M. S. Bahramy, B. Singh, C. M. Canali, T. Dietl, and C. Autieri, *Bulletin of the American Physical Society* (2023).
- [24] M. Shafiei, F. Fazileh, F. M. Peeters, and M. V. Milošević, *Physical Review Materials* **6**, 074205 (2022).
- [25] C.-Z. Chang, J. Zhang, X. Feng, J. Shen, Z. Zhang, M. Guo, K. Li, Y. Ou, P. Wei, L.-L. Wang, *et al.*, *Science* **340**, 167 (2013).
- [26] C.-Z. Chang, W. Zhao, D. Y. Kim, H. Zhang, B. A. Assaf, D. Heiman, S.-C. Zhang, C. Liu, M. H. Chan, and J. S. Moodera, *Nature materials* **14**, 473 (2015).
- [27] B. Aronzon, L. Oveshnikov, V. Prudkoglyad, Y. G. Selivanov, E. Chizhevskii, K. Kugel, I. Karateev, A. Vasiliev, and E. Lähderanta, *Journal of Magnetism and Magnetic Materials* **459**, 331 (2018).
- [28] J. Liu and T. Hesjedal, *Advanced Materials* , 2102427 (2021).
- [29] C.-Z. Chang, P. Tang, Y.-L. Wang, X. Feng, K. Li, Z. Zhang, Y. Wang, L.-L. Wang, X. Chen, C. Liu, *et al.*, *Physical Review Letters* **112**, 056801 (2014).
- [30] H. Weng, R. Yu, X. Hu, X. Dai, and Z. Fang, *Advances in Physics* **64**, 227 (2015).
- [31] A. Burkov, M. Hook, and L. Balents, *Physical Review B* **84**, 235126 (2011).
- [32] D. Son and B. Spivak, *Physical Review B* **88**, 104412 (2013).
- [33] F. Flicker, F. De Juan, B. Bradlyn, T. Morimoto, M. G. Vergniory, and A. G. Grushin, *Physical Review B* **98**, 155145 (2018).
- [34] N. B. Schröter, S. Stolz, K. Manna, F. De Juan, M. G. Vergniory, J. A. Krieger, D. Pei, T. Schmitt, P. Dudin, T. K. Kim, *et al.*, *Science* **369**, 179 (2020).
- [35] C. Fang, M. J. Gilbert, and B. A. Bernevig, *Physical Review Letters* **112**, 046801 (2014).
- [36] Y.-F. Zhao, R. Zhang, R. Mei, L.-J. Zhou, H. Yi, Y.-Q. Zhang, J. Yu, R. Xiao, K. Wang, N. Samarth, *et al.*, *Nature* **588**, 419 (2020).
- [37] C.-Z. Chang, W. Zhao, D. Y. Kim, P. Wei, J. K. Jain, C. Liu, M. H. Chan, and J. S. Moodera, *Physical Review Letters* **115**, 057206 (2015).
- [38] M. Shiranzaei, F. Parhizgar, J. Fransson, and H. Cheraghchi, *Physical Review B* **95**, 235429 (2017).
- [39] We adopt the notation such that the surface state gap is twice the exchange field.
- [40] I. Lee, C. K. Kim, J. Lee, S. J. Billinge, R. Zhong, J. A. Schneeloch, T. Liu, T. Valla, J. M. Tranquada, G. Gu, *et al.*, *Proceedings of the National Academy of Sciences* **112**, 1316 (2015).
- [41] P. Haazen, J.-B. Laloë, T. Nummy, H. Swagten, P. Jarillo-Herrero, D. Heiman, and J. Moodera, *Applied Physics Letters* **100**, 082404 (2012).
- [42] W. Liu, D. West, L. He, Y. Xu, J. Liu, K. Wang, Y. Wang, G. Van Der Laan, R. Zhang, S. Zhang, *et al.*, *ACS Nano* **9**, 10237 (2015).
- [43] R.-L. Chu, J. Shi, and S.-Q. Shen, *Physical Review B* **84**, 085312 (2011).
- [44] M. Shafiei, F. Fazileh, F. M. Peeters, and M. V. Milošević, *Physical Review B* **106**, 035119 (2022).
- [45] I. Aguilera, C. Friedrich, and S. Blügel, *Physical Review B* **100**, 155147 (2019).
- [46] S. M. Young, S. Chowdhury, E. J. Walter, E. J. Mele, C. L. Kane, and A. M. Rappe, *Physical Review B* **84**, 085106 (2011).
- [47] R. Battilomo, N. Scopigno, and C. Ortix, *Physical Review B* **100**, 115131 (2019).
- [48] Y. Liu, Y. Li, S. Rajput, D. Gilks, L. Lari, P. Galindo, M. Weinert, V. Lazarov, and L. Li, *Nature Physics* **10**, 294 (2014).
- [49] C. Richardson, J. Devine-Stoneman, G. Divitini, M. Vickers, C.-Z. Chang, M. Amado, J. Moodera, and J. Robinson, *Scientific reports* **7**, 12061 (2017).
- [50] M. Ohring, *Materials science of thin films* (Elsevier, 2001).
- [51] H. Aramberri and M. C. Muñoz, *Physical Review B* **95**, 205422 (2017).
- [52] M. R. Brems, J. Paaske, A. M. Lunde, and M. Willatzen, *Physical Review B* **97**, 081402 (2018).
- [53] M. R. Brems, J. Paaske, A. M. Lunde, and M. Willatzen, *New Journal of Physics* **20**, 053041 (2018).
- [54] W. A. Harrison, *Elementary electronic structure (revised edition)* (World Scientific Publishing Company, 2004).
- [55] Y. Jiang, Y. Sun, M. Chen, Y. Wang, Z. Li, C. Song, K. He, L. Wang, X. Chen, Q.-K. Xue, *et al.*, *Physical Review Letters* **108**, 066809 (2012).
- [56] Since the change of the volume of the sample related to the applied strain in the range [-6%,6%] is below 4.5%, we consider the magnetization to be constant, even though the concentration of magnetic dopants is strictly speaking not fixed per unit volume.
- [57] L. Bao, W. Wang, N. Meyer, Y. Liu, C. Zhang, K. Wang, P. Ai, and F. Xiu, *Scientific Reports* **3**, 2391 (2013).
- [58] S. Datta, *Electronic transport in mesoscopic systems* (Cambridge University Press, 1997).
- [59] V. Nam Do, V. H. Nguyen, P. Dollfus, and A. Bournel, *Journal of Applied Physics* **104**, 063708 (2008).
- [60] X. Feng, Y. Feng, J. Wang, Y. Ou, Z. Hao, C. Liu, Z. Zhang, L. Zhang, C. Lin, J. Liao, *et al.*, *Advanced Materials* **28**, 6386 (2016).
- [61] Q. L. He, L. Pan, A. L. Stern, E. C. Burks, X. Che, G. Yin, J. Wang, B. Lian, Q. Zhou, E. S. Choi, *et al.*, *Science* **357**, 294 (2017).
- [62] J. Wang, Q. Zhou, B. Lian, and S.-C. Zhang, *Physical Review B* **92**, 064520 (2015).